Preassembly of Membrane-Active Peptides Is an Important Factor in Their Selectivity toward Target Cells†

Neta Sal-Man, Ziv Oren, and Yechiel Shai*

Department of Biological Chemistry, Weizmann Institute of Science, Rehovot 76100, Israel

Received April 30, 2002; Revised Manuscript Received July 2, 2002

ABSTRACT: Membrane-active peptides comprise a large group of toxins used in the defense and offense systems of all organisms including plants and humans. They act on diverse targets including microorganisms and mammalian cells, but the factors that determine their target cell selectivity are not yet clear. Here, we tested the role of peptide length and preassembly on the ability of diastereomeric cationic antimicrobial peptides to discriminate among bacteria, erythrocytes, and fungal cells, by using peptides with variable lengths (13, 16, and 19 amino acids long) and their covalently linked pentameric bundles. All the bundles expressed similar potent antifungal activity (minimal inhibitory concentration of 0.2−0.3 μM) and high antimicrobial activity. Hemolytic activity was also observed at concentrations higher than those required for antifungal activity. In contrast, all the monomers showed length-dependent antimicrobial activity, were less active toward bacteria and fungi, and were devoid of hemolytic activity. BIAcore biosensor experiments revealed a ∼300-fold increase in peptide−membrane binding affinity between the 13- and 19-residue monomers toward zwitterionic (egg phosphatidylcholine (PC)/egg spingomyelin (SM)/cholesterol) vesicles. All the monomeric peptides display a similar high affinity to negatively charged (*E. coli* phosphatidylethanolamine (PE)/egg phosphatidylglycerol (PG)) vesicles regardless of their length. In contrast, irrespective of the size of the monomeric subunit, all the bundles bind irreversibly and strongly disrupt both PC/SM/cholesterol and PE/PG membranes. Attenuated total reflectance Fourier-transform infrared spectroscopy revealed that peptide assembly also affects structure as observed by an increased α-helical and β-sheet content in membranes and enhances acyl chain disruption of PC/cholesterol. The correlation between the antibacterial activity and ability to depolarize the transmembrane potential of *E. coli* spheroplasts, as well as the ability to induce calcein release from vesicles, suggests that the bacterial membrane is their target. The data demonstrate that preassembly of cationic diastereomeric antimicrobial peptides is an essential factor in their membrane targeting.

Membrane-active peptides comprise a large group of toxins used in the defense and offense systems of all organisms, including plants and humans. They lyse a variety of microorganisms and cells including bacteria as well as fungal, normal, and cancer cells. These peptides serve as a nonspecific defense system that complements the highly specific cell-mediated immune response. A major group includes positively charged amphipathic peptides, most of which act predominantly on bacteria (*1*−*6*). Although the details of their mode of action might be different, many of these peptides are believed to specifically kill bacteria by directly interacting with and disrupting the negatively charged bacterial membrane, but not the zwitterionic membrane of mammalian cells (*7*−*14*). However, despite similarities in the structure and amino acid composition of many antimicrobial peptides, their spectra of activities are different. Some are active predominantly on bacteria, and others on bacteria, fungi, and/or mammalian cells. Factors that affect cell selectivity are not yet clear.

Recent studies have suggested that the preassembly of antimicrobial peptides in solution and/or in membranes influences target cell specificity (*15*−*19*). However, the role of peptide assembly in determining cell selectivity has been traditionally studied by comparing peptides from different families or by mutating the peptide backbone. It should be noted that any differences in peptide sequences could also possibly contribute to activity and selectivity. Here, we investigated antimicrobial peptides both in their monomeric form and when linked together covalently with an inert template. For this purpose we chose de-novo-designed diastereomeric peptides (containing L- and D-amino acids) because they are highly selective to bacteria and remain predominantly as monomers in solution (*18, 20*).

The monomers were composed of 13, 16, and 19 amino acids, and each corresponding bundle was composed of five monomeric subunits (Figure 1). The rationale for using pentamers was based on the prediction of many models that at least 4−5 peptide monomers are required to form a pore in the target membrane. The peptides were investigated for their biological function, their binding to membranes composed of zwitterionic and negatively charged phospholipids by using a BIAcore biosensor, their structure in membranes, and their ability to perturb the lipid order by using ATR-

† This research was supported by European Community Project Number QLK2-2000-00411. Y.S. is the Harold S. and Harriet B. Brady Professorial Chair in Cancer Research.

* To whom correspondence should be addressed. Phone: 972-8-9342711. Fax: 972-8-9344112. E-mail: Yechiel.Shai@weizmann.ac.il.

10.1021/bi0260482 CCC: $22.00
Published on Web 08/24/2002

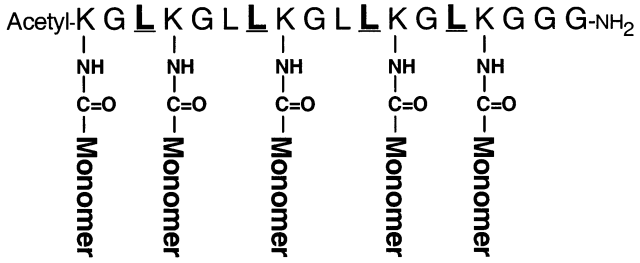

FIGURE 1: Schematic image of the bundled peptides. Each peptide is composed of a linker and five monomers.

FTIR[1] spectroscopy. They were also tested for their ability to increase the permeability of model membranes and intact bacteria. The role of peptide preassembly in determining target cell specificity is discussed on the basis of the data presented.

MATERIALS AND METHODS

Materials. Rink amide MBHA resin, 4-methylbenzhydrylamine resin (BHA), and 9-fluorenylmethoxycarbonyl (F-moc) amino acids were obtained from Calbiochem-Novabiochem AG (Switzerland). Other reagents used for peptide synthesis included trifluoroacetic acid (TFA; Sigma), piperidine (Merck), *N*,*N*-diisopropylethylamine (DIEA; Sigma), *N*-hydroxybenzotriazole hydrate (HOBT; Aldrich), 2-(1*H*-benzotriazol-1-yl)-1,1,3,3-tetramethyluronium hexafluorophosphate (HBTU), and dimethylformamide (DMF; peptide synthesis grade, Biolab). Egg phosphatidylcholine (PC), egg phosphatidylglycerol (PG), egg sphingomyelin (SM), phosphatidylethanolamine (PE) (type V, from *Escherichia coli*), cholesterol (extra pure) *N*-octyl β-D-glucopyranoside (OG), and bovine serum albumin (BSA) were purchased from Sigma. Calcein was purchased from Molecular Probes (Junction City, OR). Amphotericin B was purchased from Sigma Chemical Co. (Israel). All other reagents were of analytical grade. Buffers were prepared in double-distilled water (DDW).

Peptide Synthesis and Purification. The monomers were synthesized by the F-moc solid-phase method on a Rink amide MBHA resin, using an ABI 433A automatic peptide synthesizer. The linker of the bundled monomers was also synthesized by using the F-moc method, however on BHA, which requires hydrogen fluoride (HF) treatment for peptide cleavage. To create a bundle of monomers, the linker peptide was treated with acetic anhydride to block the N-terminus amino group, and then treated with TFA to remove the *t*-Boc protecting groups of the five lysines. Parallel synthesis of five monomers was performed on the free side chain amino group of the lysines by using the F-moc method. The monomers were cleaved from the resin by trifluoroacetic acid (TFA:DDW:TES = 18.5:1:0.5 v/v), and the bundled peptides were cleaved from the resin by HF. Each crude peptide contained one major peak, as revealed by RP-HPLC, which was 60−80% pure peptide by weight. The peptides were further purified by RP-HPLC on a C_{18} reversed-phase Bio-Rad semipreparative column (250 × 10 mm, 300 Å pore size, 5 μm particle size). The column was eluted over the course of 50 min, using a linear gradient of 15−45% and 23−50% acetonitrile in water (all containing 0.05% TFA (v/v), at a flow of 1.8 mL/min) for the monomers and bundles, respectively. The purified peptides were homogeneous (>98%) by analytical HPLC. The peptides were further subjected to amino acid analysis and electrospray mass spectroscopy to confirm their composition and molecular weight.

Preparation of Liposomes. Small unilamellar vesicles (SUVs) were prepared by sonication of PC/SM/cholesterol (5:5:1 w/w), or PE/PG (7:3 w/w) dispersions. Briefly, dry lipid mixtures were dissolved in $CHCl_3$/MeOH (2:1 v/v). The solvents were then evaporated under a nitrogen stream, and the lipids (at a concentration of 7.2 mg/mL) were subjected to a vacuum for 1 h and then were resuspended in the appropriate buffer, by vortexing. The resulting lipid dispersions were sonicated (10−30 min) in a bath-type sonicator (G1125SP1 sonicator, Laboratory Supplies Co., Inc., New York) until the turbidity had cleared. Vesicles were visualized by electron microscopy (JEOL, Tokyo, Japan) and were shown to be unilamellar, with an average diameter of 20−40 nm.

Antibacterial Activity of the Peptides. The antibacterial activity of the peptides was examined in sterile 96-well plates (Nunc F96 microtiter plates) in a final volume of 100 μL as follows: Aliquots (50 μL) of a suspension containing bacteria at a concentration of 106 colony-forming units (CFUs)/mL in culture medium (LB medium) were added to 50 μL of water containing the peptide in serial 2-fold dilutions in water. Inhibition of growth was determined by measuring the absorbance at 492 nm with a Microplate autoreader El309 (Bio-tek Instruments), after an incubation of 18−20 h at 37 °C. Antibacterial activities were expressed as the minimal inhibitory concentration (MIC), the concentration at which 100% inhibition of growth was observed after 18−20 h of incubation. The bacteria that were used included two Gram-negative and two Gram-positive species: *E. coli* D21, *Acinetobacter baumannii* ATCC 19606, *Staphylococcus aureus* ATCC 6538p, and *Enterobacter cloacae* ATCC 49141. Controls for zero antibacterial activity (blank) and high antibacterial activity consisted of bacteria suspended in LB and 100 μg/μL gentamicin in serial 2-fold dilutions, respectively.

Antifungal Activity. The antifungal activity of the peptides was examined in sterile 96-well plates (Nunc F96 microtiter plates) in a final volume of 100 μL as follows: 50 μL of a suspension containing the opportunistic fungi *Cryptococcus neoformans* at a concentration of 2×10^3 CFUs/mL in culture medium (RPMI 1640, 0.165 M MOPS, pH 7.0, with L-glutamine, without $NaHCO_3$ medium) was added to 50 μL of water containing the peptide in serial 2-fold dilutions. The fungi were incubated for 72 h at 35 °C using a Binder KB115 incubator. Growth inhibition was determined by measuring the absorbance at 620 nm in a Microplate autoreader El309

[1] Abbreviations: ATR-FTIR, attenuated total reflectance Fourier-transform infrared; OD, optical density; BHA, 4-methylbenzhydrylamine resin; Boc, butyloxycarbonyl; HF, hydrogen fluoride; diS-C_3-5, 3,3′-diethylthiodicarbocyanine iodode; HEPES, *N*-(2-hydroxyethyl)piperazine-*N*′-2-ethanesulfonic acid; hRBCs, human red blood cells; MIC, minimal inhibitory concentration; CFUs, colony-forming units; PBS, phosphate-buffered saline; PC, egg phosphatidylcholine; PE, *E. coli* phosphatidylethanolamine; PG, egg phosphatidylglycerol; SM, egg spingomyelin; RP-HPLC, reversed-phase high-performance liquid chromatography; SUVs, small unilamellar vesicles; TFA, trifluoroacetic acid; RU, resonance signal; SPR, surface plasmon resonance; TES, triethylsilane.

(Bio-tek Instruments). Antifungal activity was expressed as the MIC, the concentration at which 100% inhibition of growth was observed.

Hemolysis of Human Red Blood Cells. The peptides were tested for their hemolytic activity against human red blood cells (hRBCs). Fresh hRBCs were rinsed three times with PBS (35 mM phosphate buffer and 0.15 M NaCl (pH 7.3)) by centrifugation for 10 min at 800*g* and resuspended in PBS. Peptides dissolved in PBS were then added to 50 μL of a solution of the stock hRBCs in PBS to reach a final volume of 100 μL (final erythrocyte concentration 5% v/v). The resulting suspension was incubated with agitation for 60 min at 37 °C. The samples were then centrifuged at 800*g* for 10 min. The release of hemoglobin was monitored by measuring the absorbance of the supernatant at 540 nm. Controls for zero hemolysis (blank) and 100% hemolysis consisted of hRBCs suspended in PBS and 10 μg of melittin, respectively.

Membrane Permeability Studies. Calcein (60 mM, self-quenching concentration) was entrapped into vesicles composed of PC/SM/cholesterol (5:5:1w/w) or PE/PG (7:3 w/w). The buffer that was used contained 10 mM Tris solution and 150 mM NaCl, at pH 7.4. The nonencapsulated calcein was removed from the liposome suspension by gel filtration, using a Sephadex G-50 (Pharmacia) column connected to a low-pressure LC system (Pharmacia). The eluent was monitored by UV absorbance ($\lambda = 280$ nm), and the vesicles' peak was collected and diluted 10-fold in the same buffer. A final concentration of 22 μM SUV was used. Trapped inside vesicles, the calcein dye became self-quenched. Increasing membrane permeability was detected by an increase in fluorescence after the addition of a peptide ($\lambda_{ex} = 485$ nm; $\lambda_{em} = 515$ nm) (*21*). The percentage of fluorescence recovery, F_t, was defined as

$$F_t = (I_t - I_0/I_f - I_0) \times 100$$

where I_0 = the initial fluorescence, I_f = the total fluorescence observed after the maximum calcein release was achieved for each peptide, and I_t = the fluorescence observed at equilibrium, after the addition of peptide in different concentrations.

In Vivo Transmembrane Potential Depolarization Assay. A potential depolarization assay was performed with *E. coli* spheroplasts. Similar experiments have been described previously for a permeable *E. coli* mutant (*13*). Membrane destabilization, which results in the collapse of the transmembrane potential, was detected using a fluorescence dye (*22*). The dye binds the plasma membrane because of the cell transmembrane potential, resulting in a quenching of the dye's fluorescence. Peptide-induced membrane permeation caused a dissipation of the transmembrane potential that was monitored by an increase in fluorescence due to the release of the dye. More specifically, spheroplasts of *E. coli* (D21) were prepared by the osmotic shock procedure as follows: Cells from cultures grown to $OD_{600} = 0.8$ were harvested by centrifugation and washed twice with 10 mM Tris/H_2SO_4, 25% sucrose, pH 7.5. The cells were resuspended in the washing buffer containing 1 mM EDTA. After a 10 min incubation at 20 °C with rotary mixing, the cells were collected by centrifugation and resuspended immediately in cold (4 °C) water. After a 10 min incubation at 4 °C with rotary mixing, the spheroplasts were collected by centrifugation. The spheroplasts were then resuspended to an OD_{600} of 0.1 in a buffer containing 20 mM glucose, 5 mM HEPES, and 1 M KCl, pH 7.3. The cells were incubated with 1 μM diS-C_3-5 until there was no reduction of fluorescence (around 3 h), indicating the incorporation of the dye into the bacterial membrane. The experiments were performed in sterile 96-well plates (Nunc F96 microtiter plates) in a final volume of 100 μL, as follows: 50 μL of a suspension containing bacteria and the dye was added to 50 μL of the final buffer containing the peptide in serial 2-fold dilutions. Membrane depolarization was monitored by the change in the intensity of fluorescence emission of the membrane-potential-sensitive dye diS-C_3-5 (exitation wavelength $\lambda_{ex} = 622$ nm, emission wavelength $\lambda_{em} = 670$ nm) after different concentrations of peptides were added.

ATR-FTIR Measurements. Spectra were obtained with a Bruker equinox 55 FTIR spectrometer equipped with a deuterated triglyceride sulfate (DTGS) detector that was coupled to an ATR device. For each spectrum, 150 scans were collected, with resolution of 4 cm^{-1}. Samples were prepared as previously described (*23*). Briefly, a mixture of PC/cholesterol or PE/PG (0.5 mg) alone or with peptide was deposited on a ZnSe horizontal ATR prism (80 × 7 mm). The aperture angle of 45° yielded 25 internal reflections. Prior to preparing the samples, the trifluoroacetate (CF_3COO^-) counterions, which strongly associate with the peptide, were replaced with chloride ions by washing in 0.1 M HCl and lyophilization. This eliminated the strong C═O stretching absorption band near 1673 cm^{-1} (*24*). Lipid−peptide mixtures were prepared by dissolving them together in a 1:2 MeOH/CH_2Cl_2 mixture and drying them under vacuum for 15 min. Lipid−peptide mixtures or lipids were spread with a Teflon bar on the ZnSe prism. Polarized spectra were recorded, and the respective pure phospholipids in each polarization were subtracted to yield the difference spectra. The background for each spectrum was a clean ZnSe prism. Hydration of the sample was achieved by introducing an excess of deuterium oxide (D_2O) into a chamber placed on top of the ZnSe prism in the ATR casting and incubating for 15 min before acquisition of the spectra. The H/D exchange was considered complete due to a complete shift of the amide II band. Any contribution of $2H_2O$ vapor to the absorbance spectra near the amide I peak region was eliminated by subtraction of the spectra of pure lipids equilibrated with $2H_2O$ under the same conditions.

ATR-FTIR Data Analysis. Prior to curve fitting, a straight baseline passing through the ordinates at 1700 and 1600 cm^{-1} was subtracted. To resolve overlapping bands, the spectra were processed using PEAKFIT (Jandel Scientific, San Rafael, CA) software. Second-derivative spectra accompanied by 13-data-point Savitsky−Golay smoothing were calculated to identify the positions of the component bands in the spectra. These wavenumbers were used as initial parameters for curve fitting with Gaussian component peaks. The positions, bandwidths, and amplitudes of the peaks were varied until (i) the resulting bands shifted by no more than 2 cm^{-1} from the initial parameters, (ii) all the peaks had reasonable half-widths ($<20-25$ cm^{-1}), and (iii) good agreement between the calculated sum of all components and the experimental spectra was achieved ($r^2 > 0.999$). The relative contents of different secondary structure elements were estimated by dividing the areas of individual peaks,

which were assigned to a particular secondary structure, by the whole area of the resulting amide I band. The results of three independent experiments were averaged.

Binding Analysis by Using a BIAcore Biosensor. Biosensor experiments were carried out using conditions modified from what has been described recently (*25*) with a BIAcore X analytical system (Biacore, Uppsala, Sweden) using an HPA sensor chip (Biacore). The HPA sensor chip is composed of long-chain alkanethiol molecules covalently linked to a gold surface to form a hydrophobic monolayer. The running buffer used for all the experiments was PBS without Ca^{2+} and Mg^{2+} (pH 6.8). The washing solution was 40 mM *N*-octyl β-D-glucopyranoside. The monolayer can be recycled and used for the other peptides' binding studies by washing the bound peptides using 10−100 mM NaOH or HCl for 1−2 min. After this process, the baseline returned to its original level. All solutions were freshly prepared, degassed, and filtered through 0.22 μm pores. All the experiments were done at a temperature of 25 °C. After the system was cleaned according to the manufacturer's instructions, the BIAcore X instrument was left running overnight using Milli-Q water as eluent to thoroughly wash all liquid-handling parts of the instrument. The HPA chip was then installed, and the alkanethiol surface was cleaned by an injection of the nonionic detergent 40 mM *N*-octyl β-D-glucopyranoside (25 μL), at a flow rate of 5 μL/min. PC/SM/cholesterol (5:5:1 w/w) or PE/PG (7:3 w/w) vesicles (80 μL, 0.5 mM) were then applied to the chip surface at a low flow rate (2 μL/min). To remove any multilamellar structures from the lipid surface, NaOH (50 μL, 10 mM) was injected at a flow rate of 50 μL/min, which resulted in a stable baseline corresponding to the lipid monolayer linked to the chip surface. The negative control BSA was injected (25 μL, 0.1 mg/μL in PBS) to confirm complete coverage of the chip surface with lipids by the absence of nonspecific binding. This monolayer, linked to the chip surface, was then used as a model membrane surface to study the peptide−membrane binding.

In a typical experiment, peptide solutions (15 μL PBS solution of 0.1−100 μM peptide) were injected onto the lipid surface at a flow rate of 5 μL/min. PBS alone then replaced the peptide solution for 1200 s to allow for peptide dissociation. Analysis of the peptide−lipid binding event was performed from a series of sensograms collected at five different peptide concentrations (Figure 6). Surface plasmon resonance (SPR) was used to detect changes in the reflective index of the surface layer of peptides and lipids in contact with the sensor chip. A sensogram was obtained by plotting the SPR angle against time. The SPR angle is represented by the resonance signal (RU). The curve of the RU, as a function of time, displays the progress of the interaction between the peptide and the lipid monolayer at the sensor surface. The partition constants were calculated from the primary sensogram data by nonlinear fitting (*26*, *27*) using the software supplied by the manufacturer. The partition constants were derived from the following equation:

$$\mathrm{RU}(x) = \frac{KX(\mathrm{RU}_{\max})}{1 + KX}$$

where X is the peptide concentration, $\mathrm{RU}_{\max}$ is the maximal response unit, and K is the partition constant.

Table 1: Sequences and Designations of the Peptides Investigated

Peptide designation	Sequence[a,b,c]
13-mer	K L **L L** K W K **L** K **L** L K G-NH_2
16-mer	K **L** L K L **L L** K W K **L** K **L** L K G-NH_2
19-mer	K **L** L K **L** L K L **L L** K W K **L** K **L** L K G-NH_2
13-mer bundle	Linker + 5 subunits of the 13-mer
16-mer bundle	Linker + 5 subunits of the 16-mer
19-mer bundle	Linker + 5 subunits of the 19-mer
Linker[d]	Ac -*K* G **L** *K* G L **L** *K* G L **L** *K* G **L** *K* G G G-NH_2

[a] Underlined and bold amino acids are D-enantiomers. [b] The C-terminal is amidated. [c] In italics are indicated the side chains used as starting points for the synthesis of each monomer. [d] Ac = acetyl

RESULTS

Peptide Design and Sequences. Three diastereomers of linear peptides having different lengths (13, 16, and 19 amino acids) and their covalently linked bundles were synthesized and investigated. Each bundle is composed of a biologically inert linker and five subunits that have sequences identical to those of the monomers (Figure 1). All the peptides consist of positively charged (lysine) and hydrophobic (leucine) amino acids and include tryptophan, used to determine their concentration. The sequences of the peptides and their designations are given in Table 1.

Antimicrobial and Antifungal Activity of the Peptides. The peptides were studied for their potential to inhibit the growth of different microorganisms. Table 2 gives the MICs for a representative set of bacteria that includes both Gram-negative species, *E. coli* and *A. baumannii*, and Gram-positive species, *S. aureus* and *E. cloacae*, as well as one strain of opportunistic fungi, *C. neoformans*. The results are shown in Table 2. The data indicate that increasing the length, and consequently the net positive charge, of the monomers increased their activity toward both bacteria and fungi. In contrast, the antibacterial activity of all three bundles was similar and high regardless of the length of their monomeric subunit. Similarly, all the bundles had similar, very high activity toward *C. neoformans*.

Hemolytic Activity of the Peptides. The peptides were tested for the extent of their hemolytic activity against the highly susceptible human erythrocytes (5% erythrocyte solution). Figure 2 shows a dose−response curve for the hemolytic activity of the peptides. The results revealed that all the monomers, including the linker, were not hemolytic. In contrast, all the bundles, irrespective of the monomeric subunit size, were able to lyse erythrocytes, indicating that peptide preassembly has a crucial role in determining cell specificity of positively charged antimicrobial peptides. The hemolytic activity of the bee venom melittin (35 μM) served as a standard for 100% hemolysis.

Peptides Induced Calcein Leakage from Vesicles. The ability of the peptides to cause membrane leakage was studied *in vitro*, by testing their ability to evoke calcein release from SUVs composed of PC/SM/cholesterol (5:5:1 w/w), a composition that mimics the outer erythrocyte leaflet (*28*), and of negatively charged PE/PG (7:3 w/w), a phospholipid composition typical of *E. coli* (*29*). Increasing amounts of peptides were added to a 22 μM vesicle suspension. Membrane permeability was monitored by following the fluorescence recovery for 15 min. The dose

Table 2: Minimal Inhibitory Concentration (μM) of the Peptides

peptide designation	minimal inhibitory concentration[a] (μM)				
	bacteria				fungi
	E. coli (D21)	*A. baumannii* (ATCC 19606)	*S. aureus* (ATCC 6538p)	*E. cloacae* (ATCC 49141)	*C. neoformans* (ATCC MYA-422)
13-mer	16	47	63	47	12.5
13-mer bundle	4	4	8	8	0.3
16-mer	5	10	38	20	3.3
16-mer bundle	4.5	4.5	6.5	6.5	0.3
19-mer	2.5	2	11	3	1.4
19-mer bundle	2	1.5	6	4	0.2
linker	>200	>200	>200	>200	>100

[a] The results are the mean of three independent experiments each performed in duplicate, with a standard deviation of 25%.

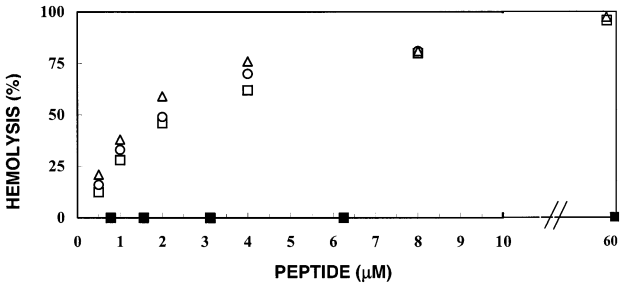

FIGURE 2: Dose−response of the hemolytic activity of the peptides toward hRBCs. The assay was performed as described in the Materials and Methods. The designations are as follows: ■, 13-mer; □, 13-mer bundle; ●, 16-mer; ○, 16-mer bundle; ▲, 19-mer; △, 19-mer bundle; ◆, linker. All black symbols are covered by squares since all full symbols fall on the baseline.

responses of the peptide-induced calcein release from the PC/SM/cholesterol and PE/PG vesicles are shown in Figures 3 and 4, respectively. Overall, the ability of all the peptides to induce calcein release from the PE/PG vesicles correlates with their antibacterial activity. Among the monomers, the 13-mer is the least active compared to the others. However, all the bundles have similar activity, in agreement with their similar and high antibacterial activity. Interestingly, the difference between a monomer and its corresponding bundle is more pronounced in the activity toward model membranes compared with intact bacteria. This can possibly be explained by taking into account the difference between the two systems. The model membranes are composed of only one layer of phospholipids, PE and PG, whereas the bacterial wall contains phospholipids, lipopolysaccharides (LPSs), and peptidoglycan layers. The bundles have a larger volume compared with the monomers, which prevents them from diffusing efficiently through the peptidoglycan or the LPS layers into the inner bacterial membrane. However, we cannot rule out the charge effect coming from the tighter electrostatic interactions between the bundles and the peptidoglycan or LPS layers.

Interestingly, the 13-mer is not active at all on PC/SM/cholesterol vesicles, whereas the 16-mer and the 19-mer are active. Despite this, all three monomers are nonhemolytic, the reason for which is explained in the Discussion. In contrast, all the bundled peptides are more active than their parental monomers on PC/SM/cholesterol vesicles, a property that correlates with their hemolytic activity. Note that a certain concentration of a bundled peptide is equivalent to a 5-fold concentration of the parental monomeric peptide. Nevertheless, even when taking this into account, the bundled peptides are more active on PC/SM/cholesterol compared

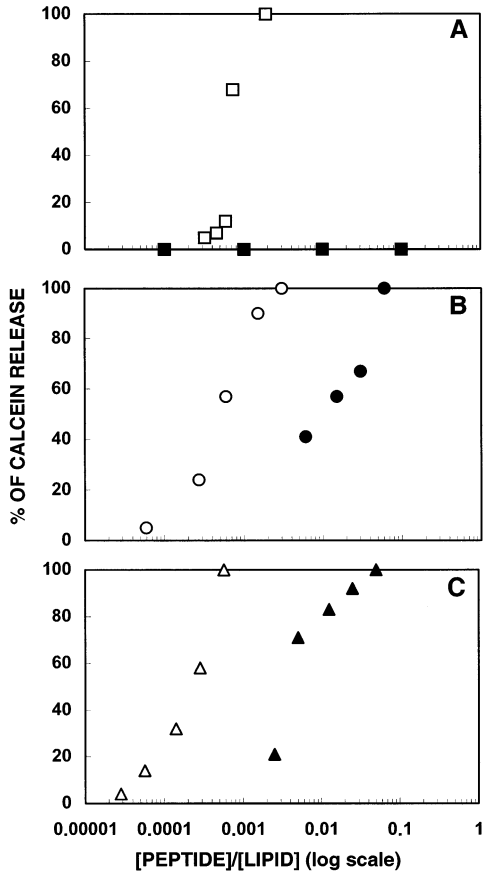

FIGURE 3: Calcein release from PC/SM/cholesterol SUVs induced by the peptides. Peptides were added to calcein-containing PC/SM/cholesterol SUVs. An increase in the fluorescence versus the molar ratio of peptide to lipid was recorded. Calcein release of 100% was normalized for each peptide. Key: panel A, 13-mer and bundle; panel B, 16-mer and bundle; panel C, 19-mer and bundle. The designations are as follows: ■, 13-mer; □, 13-mer bundle; ●, 16-mer; ○, 16-mer bundle; ▲, 19-mer; △, 19-mer bundle.

to their parental monomers (Figure 3). However, with PE/PG vesicles the activities become similar. This indicates a synergistic effect of the bundled peptides toward PC/SM/cholesterol vesicles but not for PE/PG vesicles. Furthermore, the finding of a similar potency in increasing the permeability of PE/PG vesicles by the monomers and the bundles (when their concentration is calculated per a monomeric unit), together with the estimation of the number of monomers required for initial activity, as has been described previously (*23*), supports the notion that the first stage in their mode of action is to cover the surface of the bacterial membrane, as described in the "carpet" model.

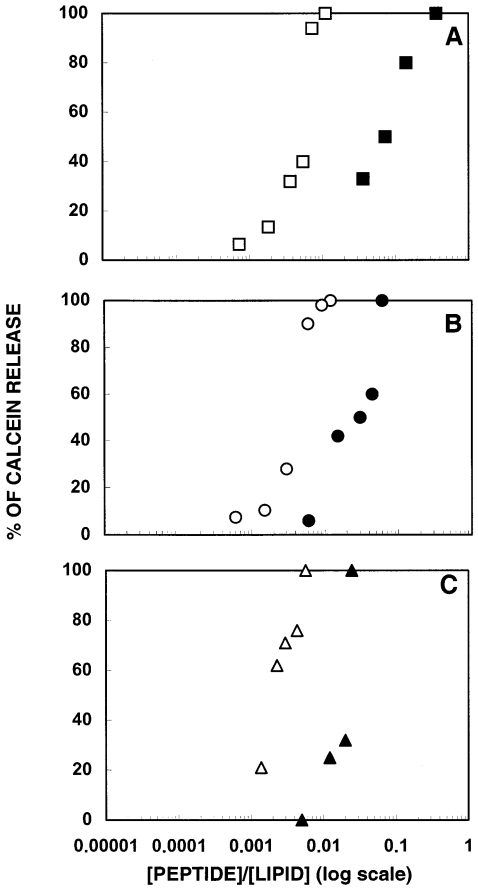

FIGURE 4: Calcein release from PE/PG SUVs induced by the peptides. Peptides were added to calcein-containing PE/PG SUVs. The increase in the fluorescence versus the molar ratio of peptide to lipid was recorded. Details are as described in the caption of Figure 3.

Transmembrane Potential Depolarization of E. coli Spheroplasts. We have used an *in vivo* potential depolarization assay similar to what has been described for a permeable mutant of *E. coli* (*13*), but used *E. coli* spheroplasts that lack the outer layer, instead. We found that the bundles are more active (Figure 5) and act with a faster kinetics (data not shown) than the monomers, similar to what has been found with PE/PG membranes. Overall, the order of activity toward *E. coli* spheroplasts but not toward intact bacteria correlates with the activity toward PE/PG membranes. These data support our assumption that the decreased activity of the bundles toward intact bacteria results from difficulties of the bundled peptides in reaching the inner membrane.

Affinity of the Peptides to Lipid Monolayers of Different Compositions As Determined by a BIAcore Biosensor. The PC/SM/cholesterol (5:5:1 w/w) and PE/PG (7:3 w/w) monolayers were absorbed onto an HPA chip. Typical sensograms of the binding of the monomeric peptides and their bundles to monolayers of PC/SM/cholesterol are shown in parts A and B of Figures 6, respectively. The sensograms for PE/PG (7:3 w/w) were similar to those observed with PC/SM/cholesterol and therefore are not shown. The peptide concentrations used for the monomers were 12.5, 25, 50, and 100 μM, and for the bundles 0.25, 0.5, 1, 2, and 5 μM. The RU signal intensity increased as a function of the peptides' concentrations, indicating that the amount of peptide bound to the lipids is proportional to the increase in peptide concentration. Since the bundled peptides were bound

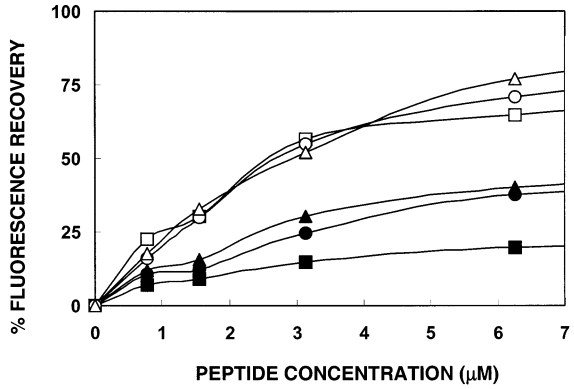

FIGURE 5: Depolarization of the membrane potential of *E. coli*. Membrane destabilization, which results in the collapse of a transmembrane potential, was detected fluorimetrically using a fluorescence dye. A suspension containing *E. coli* spheroplasts and the dye (50 μL) was added to 50 μL of buffer containing the peptides in serial 2-fold dilutions. Membrane depolarization was monitored by an increase in the fluorescence of diS-C_3-5 (excitation wavelength λ_{ex} = 622 nm, emission wavelength λ_{em} = 670 nm) after the addition of peptides at different concentrations. The designations are as follows: ■, 13-mer; □, 13-mer bundle; ●, 16-mer; ○, 16-mer bundle; ▲, 19-mer; △, 19-mer bundle.

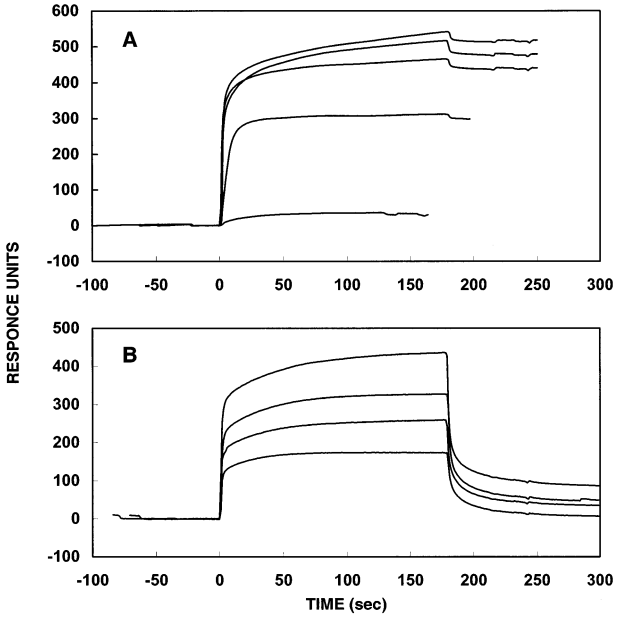

FIGURE 6: Sensograms of the binding between the monolayers—PC/SM/cholesterol (5:5:1 w/w)—and various concentrations of the 19-mer bundle (panel A) and the 19-mer monomer (panel B). Panel A shows the 19-mer bundle at concentrations of 0.25, 0.5, 1, 2, 3.75, and 7.5 μM and panel B the monomer at concentrations of 12.5, 25, 50, 100, and 200 μM. An increase in binding as the peptide concentration increases is also shown.

irreversibly to the lipid monolayer, the partition constants were calculated only for the monomers. With the monomers, equilibrium was reached during sample injection; therefore, the partition constants could be calculated from the relationship between the equilibrium binding response (R_{eq}) and the peptide concentration (Figure 7), using a steady-state affinity model. The partition constants (Table 3) are defined as the ratios of the association and dissociation rate constants ($K_A = k_a/k_d$). The data reveal an order of magnitude increase in the partitioning of the peptides to PC/SM/cholesterol for every three amino acid increase in size. Interestingly, however, independent of the peptide size, all the monomers

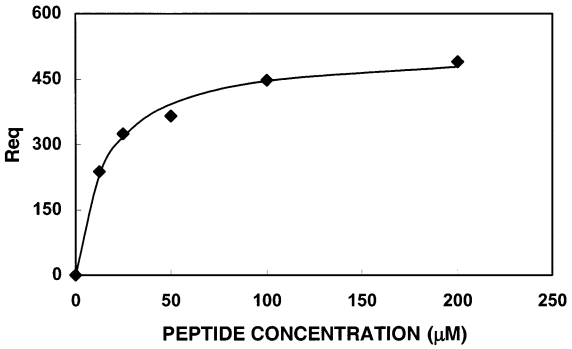

FIGURE 7: Relationship between the equilibrium binding response (R_{eq}) in PE/PG (7:3 w/w) and the peptide (19-mer) concentration using the BIAcore steady-state affinity model.

Table 3: Partition Constants and Free Energy of Binding of the Peptides to Phospholipid Membranes

	PC/SM/cholesterol		PE/PG	
peptide designation	K_A[a] (M^{-1})	$-\Delta G$[b] (kcal/mol)	K_A (M^{-1})	$-\Delta G$ (kcal/mol)
13-mer	0.7×10^2	4.87	4.0×10^4	8.62
16-mer	2.3×10^3	6.93	1.0×10^4	7.80
19-mer	1.8×10^4	8.14	6.5×10^4	8.90

[a] The results are the mean of three independent experiments with a standard deviation of 5%. [b] $\Delta G = -RT \ln 55.5K_A$.

have similar, high affinity to (PE/PG) membranes. In contrast to the reversible binding of the monomers to both types of membranes, all the bundles bind strongly and irreversibly to these membranes, which correlates with their high potency in the calcein release assay.

Secondary Structure of the Peptides in PE/PG and PC/Cholesterol Phospholipid Membranes As Determined by Using FTIR Spectroscopy. FTIR spectroscopy was used to determine the secondary structure of the peptides within the phospholipid membranes. With FTIR spectroscopy, helical and unordered structures can contribute to the amide I vibration at almost identical wavenumbers, and it is difficult to determine the precise proportion of helix and random coil structures from the IR spectra. However, the exchange of hydrogen with deuterium makes it sometimes possible to differentiate α-helical components from a random structure, since the random structure absorption shifts to a higher extent than the α-helical component after deuteration. Therefore, we examined the IR spectra of the peptides after complete deuteration. SM could not be used for FTIR studies due to the amide bond absorbance in the amide I region; thus, for zwitterionic membranes, we studied the structure of the peptides in PC/cholesterol without SM. The spectra of the amide I region of the 16-mer bundle and the 16-mer monomer bound to the PE/PG (7:3 w/w) multibilayers are shown in Figures 8 and 9, respectively. The profiles of all the monomers and bundles were quite similar to the profiles of the 16-mer and 16-mer bundle, respectively, and therefore are not shown. The spectra of the amide I region of the peptides bound to PC/cholesterol (10:1 w/w) were similar to those observed with PE/PG and therefore are also not shown. Second derivatives accompanied by 13-data-point Savitsky−Golay smoothing were calculated to identify the positions of the component bands in the spectra and are given in the corresponding panels in Figures 8 and 9. These wavenumbers were used as initial parameters for curve fitting

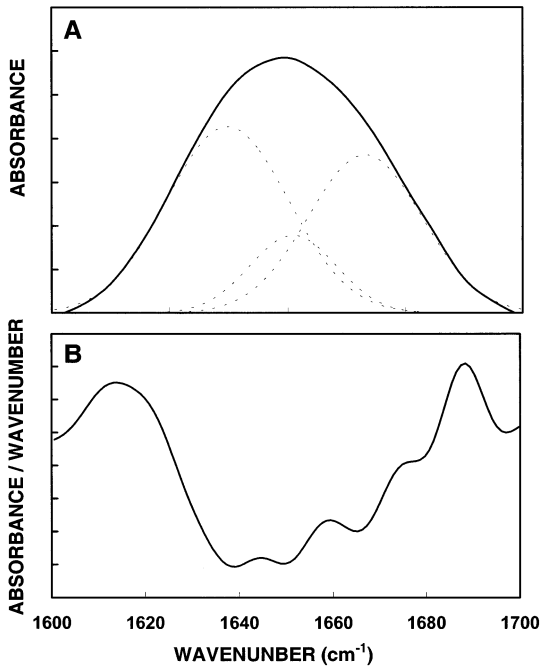

FIGURE 8: FTIR spectral deconvolution of the fully deuterated amide I band (1600−1700 cm^{-1}) of the 16-mer bundle (panel A) in PE/PG (7:3 w/w) multibilayers. The second derivatives, calculated to identify the positions of the component bands in the spectra, are shown in panel B for the 16-mer bundle. The component peaks are the result of curve fitting using a Gaussian line shape. The amide I frequencies characteristic of the various secondary structure elements were taken from ref *30*. The sums of the fitted components are superimposed on the experimental amide I region spectra. In panel A, the continuous lines represent the experimental FTIR spectra after Savitzky−Golay smoothing; the broken lines represent the fitted components. A 1:30 peptide:lipid molar ratio was used.

with Gaussian component peaks. The assignments, wavenumbers (ν), and relative areas of the component peaks are summarized in Tables 4 and 5.

Assignment of the different secondary structures to the various amide I regions was calculated according to the values taken from Jackson and Mantsch (*30*). The amide I region from 1625 to 1640 cm^{-1} is characteristic of a β-sheet structure, whereas the amide I region of an α-helical structure is located between 1650 and 1655 cm^{-1} (*31*). The amide I region from 1656 to 1670 cm^{-1} is characteristic of a 3_{10}-helix/dynamic helix (*31*) or a distorted helix (*24*, *32*−*34*). The assignment of the amide region between 1670 and 1680 cm^{-1} remains uncertain. Previous studies have correlated this region with β-turns (*35*), possibly sterically constrained non-hydrogen-bonded amide C═O groups within turns (*36*), or the high-frequency β-sheet component (*37*), which arises as a result of transition dipole coupling (*38*). The data reveal similar structures for the 13-mer and the 16-mer monomers (∼40% dynamic helix and ∼60% random coil) in PC/cholesterol membranes. Under similar conditions the random coil fraction became partially α-helical (17%) with partially β-sheet structures in the 19-mer. When bound to PE/PG membranes, all the monomers adopt a 30%−50% dynamic helix and a 50%−70% random coil. In contrast to the monomers, all the bundled peptides adopt similar structures in both PE/PG and PC/cholesterol. Their structural components are ∼45% β-sheet, ∼20% α-helix, and ∼35% dynamic helix. Structural changes between a monomeric and an

Table 4: Assignments, Wavenumbers (ν), and Relative Areas of the Component Peaks Determined from the Deconvolution of the Amide I Bands of the Peptides Incorporated into PE/PG (7:3 w/w) Multibilayers[a]

	random coil		α-helix		dynamic/3_{10}-helix		β-sheet/turn	
peptide designation	ν (cm^{-1})	area (%)	ν (cm^{-1})	area (%)	ν (cm^{-1})	area (%)	ν (cm^{-1})	area (%)
13-mer	1642 ± 1	50 ± 4			1662 ± 2	48 ± 4		
16-mer	1643 ± 1	70 ± 7			1666 ± 1	30 ± 7		
19-mer	1642 ± 1	63 ± 4			1665 ± 1	35 ± 4		
13-mer bundle			1650 ± 1	14 ± 3	1662 ± 1	37 ± 2	1637 ± 1	47 ± 3
16-mer bundle			1650 ± 1	14 ± 1	1667 ± 1	37 ± 2	1638 ± 1	48 ± 1
19-mer bundle			1650 ± 1	13 ± 1	1667 ± 1	34 ± 2	1637 ± 1	50 ± 3

[a] A 1:30 peptide:lipid molar ratio was used. All values are given as means ± standard error. The results are the mean of three independent experiments.

Table 5: Assignments, Wavenumbers (ν), and Relative Areas of the Component Peaks Determined from the Deconvolution of the Amide I Bands of the Peptides Incorporated into PC/Cholesterol (10:1 w/w) Multibilayers[a]

	random coil		α-helix		dynamic/3_{10}-helix		β-sheet/turn	
peptide designation	ν (cm^{-1})	area (%)	ν (cm^{-1})	area (%)	ν (cm^{-1})	area (%)	ν (cm^{-1})	area (%)
13-mer	1643 ± 1	57 ± 1			1667 ± 1	41 ± 1		
16-mer	1642 ± 1	56 ± 1			1667 ± 1	42 ± 1		
19-mer			1650 ± 1	17 ± 1	1667 ± 1	42 ± 1	1637 ± 2	39 ± 1
13-mer bundle			1651 ± 1	20 ± 3	1667 ± 1	36 ± 2	1636 ± 1	42 ± 1
16-mer bundle			1651 ± 1	17 ± 3	1667 ± 1	33 ± 2	1637 ± 1	48 ± 1
19-mer bundle			1650 ± 1	16 ± 1	1667 ± 1	36 ± 1	1636 ± 1	46 ± 1

[a] A 1:30 peptide:lipid molar ratio was used. All values are given as means ± standard error. The results are the mean of three independent experiments.

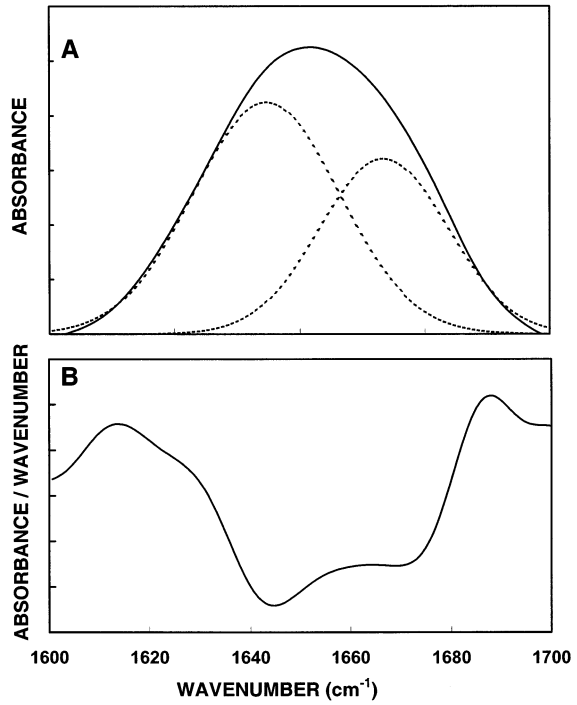

FIGURE 9: FTIR spectral deconvolution of the fully deuterated amide I band (1600−1700 cm^{-1}) of the 16-mer (A) in PE/PG (7:3 w/w) multibilayers and its second derivative (B). Details are as described in the caption of Figure 8. A 1:30 peptide:lipid molar ratio was used.

oligomeric form of a particular peptide are known to occur with natural peptides.

Orientation of the Phospholipid Membrane and the Effect of the Peptides on the Phospholipid Acyl Chain Order. Polarized ATR-FTIR spectroscopy was used to determine the orientation of the lipid membrane. The symmetric [$\nu_{sym}(CH_2) \approx 2853\ cm^{-1}$] and the antisymmetric [$\nu_{sym}(CH_2) \approx 2922\ cm^{-1}$] vibrations of lipid methylene C−H bonds are perpendicular to the molecular axis of a fully extended hydrocarbon chain. Thus, measurements of the dichroism of infrared light absorbance can reveal the order and orientation of the membrane sample relative to the prism surface. The effect of the peptides on the acyl chain order was estimated by comparing the CH_2 stretching dichroic ratio of pure phospholipid multibilayers with that obtained with membrane-bound peptide (Figure 10), and the calculated values of these ratios are given in Table 6. The data reveal that the incorporation of the bundles has a significantly higher effect on the acyl chain order of PC/cholesterol membranes compared with the incorporation of the monomers, in agreement with the hemolytic activity of the bundles (Figure 2). However, both the monomers and the bundles have a similar, high effect on PE/PG membranes, in agreement with their high capacity to permeate PE/PG vesicles and *E. coli* spheroplasts (Figures 4 and 5).

DISCUSSION

An interesting finding in this study is that preassembly of antimicrobial peptides makes them highly active on *C. neoformans*. We chose a new family of diastereomeric peptides that would form an amphipathic α-helix in their L-amino acid form, as predicted by the Schiffer and Edmundson wheel structure (*39*) (figure not shown). The advantage of this group is that they are predominantly monomers in solution and in membranes, and have selective activity toward bacteria compared with all L-amino acid counterparts (*17*, *20*, *40*). Furthermore, the presence of a few D-amino acids within their sequence gives them several therapeutic advantages, such as preserving biological activity in serum (*41*), and the possibility of controlling enzymatic

Table 6: Dichroic Ratios of the Phospholipid Multibilayers[a]

peptide	dichroic ratio of $\nu_{antisym}(CH_2)$ PC/cholesterol	dichroic ratio of $\nu_{antisym}(CH_2)$ PE/PG	peptide	dichroic ratio of $\nu_{antisym}(CH_2)$ PC/cholesterol	dichroic ratio of $\nu_{antisym}(CH_2)$ PE/PG
phospholipid	1.22 ± 0.02	1.29 ± 0.03	13-mer bundle	1.43 ± 0.02	1.40 ± 0.01
13-mer	1.30 ± 0.04	1.33 ± 0.02	16-mer bundle	1.42 ± 0.03	1.40 ± 0.01
16-mer	1.29 ± 0.02	1.36 ± 0.02	19-mer bundle	1.56 ± 0.02	1.55 ± 0.05
19-mer	1.31 ± 0.02	1.40 ± 0.03			

[a] A 1:30 peptide:lipid molar ratio was used.

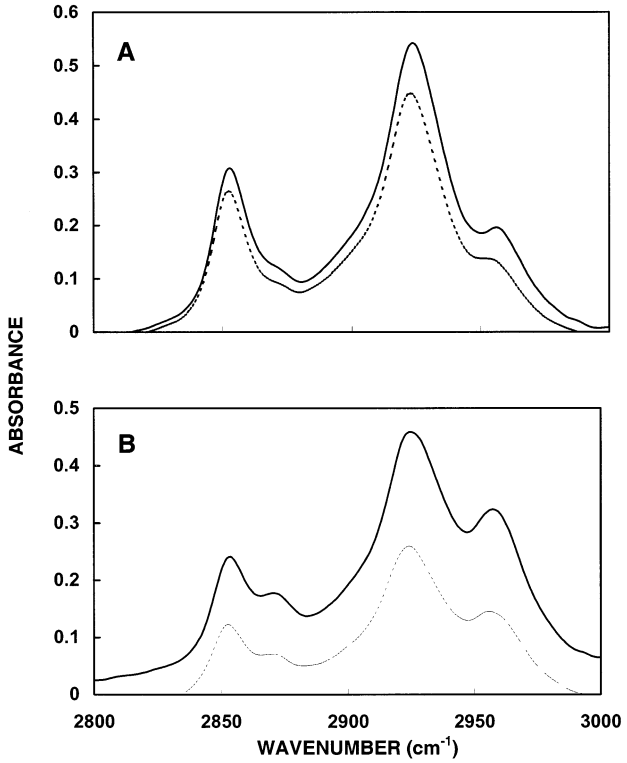

FIGURE 10: ATR dichroism spectra of parallel and perpendicularly polarized ATR-FTIR absorbance spectra between 3000 and 2800 cm^{-1} for the lipid CH_2 symmetric and antisymmetric vibration of PC/cholesterol (10:1 w/w) multibilayers alone (A) or incorporated with the 19-mer bundle (B). The top line is for the parallel component, and the bottom line is for the perpendicular component.

degradation by placing the D-amino acids at selected sites that are sensitive to degradation.

Effect of Preassembly on Antimicrobial Activity and the Ability To Permeate Negatively Charged Membranes and E. coli Spheroplasts. The antibacterial activity of the monomers increased as the length of the peptides increased. This trend in their activity correlates with the order of activity in the calcein release experiments, showing maximum activities at peptide:lipid molar ratios of 0.30, 0.08, and 0.02 for the monomeric 13-mer, 16-mer, and 19-mer, respectively. However, all the bundles have potent and similar antimicrobial activity independent of the size of the monomers. Furthermore, the calcein release activities of all the bundles are also similar. A correlation between the antimicrobial activities and the ability to dissipate the transmembrane potential of *E. coli* spheroplasts was also noted (Figure 5). The order of activities found is

$$\text{13-mer bundle} = \text{16-mer bundle} = \text{19-mer bundle} > \text{19-mer} > \text{16-mer} > \text{13-mer}$$

This correlation supports the notion that the target of these peptides is the bacterial membrane. Note that recent reports suggest that a number of cationic peptides can traverse intact membranes to interact with internal targets rather than lysing the bacterial membranes (*42*).

We also found a direct correlation between the increased antimicrobial activity (Table 2) and the increased effect of the monomers on the acyl chain order of PE/PG membranes as a result of peptide length extension (Table 6). Furthermore, in agreement with their similar antimicrobial activity, all the bundles have a similar effect on the acyl chain order.

Effect of Preassembly on Antifungal Activity and the Ability To Permeate Zwitterionic Membranes. We found that the bundled peptides have very high antifungal activity. They are up to 40-fold more potent toward *C. neoformans* compared with the monomeric forms (Table 2). Furthermore, preassembly also increases their activity toward erythrocytes. These results are in agreement with the greater effect of all the bundles on the PC/cholesterol membrane acyl chain order compared with that of their parental monomers. Furthermore, whereas the affinity of the monomeric peptides to zwitterionic phospholipids is either lower than or similar to that of many native antimicrobial peptides, all the bundles bound irreversibly to these membranes (BIAcore studies, Figure 6). Since the peptides have a high net positive charge, it is reasonable to assume that hydrophobic interactions are predominantly involved between the peptides and the zwitterionic phospholipids. According to the FTIR results, the bundled peptides form more organized amphipathic structures than the monomers (α-helix and β-sheet), which could mediate better binding to the membrane. The results of the calcein release assay also correlate well with the antifungal and hemolytic assays and the BIAcore studies. The bundles are highly active toward PC/SM/cholesterol vesicles compared with the monomers. In the calcein release assay the 13-mer is not active, even at high [peptide]:[lipid] molar ratios (up to 1.43); however, the 16-mer and 19-mer show partial activity although they are not active at all against hRBCs. A possible explanation for this difference may involve the way in which the different peptides interact with the membrane. Both monomers and bundles attach first to the glycocalix layer (negatively charged sialic acid-containing carbohydrates in the form of glycoproteins and glycosphingolipids) of the hRBCs because of their negative charge. This should make it more difficult for the monomers to partition into the cell PC membrane compared with a situation in which they partition into the membrane directly from the solution. Since the bundles bind irreversibly to PC membranes, they can shift the equilibrium from the glycocalix layer to the erythrocyte membrane and therefore become hemolytic.

Preassembly Changes the Random Coil Fraction of the Monomers to α-Helical and β-Sheet Structures. The results

of the ATR-FTIR studies revealed that all the monomers, besides the 19-mer in PC/cholesterol, adopt similar structures in both zwitterionic and negatively charged membranes (50−70% random coil and 30−50% dynamic helix). Compared to those of the monomers, the structures of the bundles did not include any random coil fraction. This fraction (∼60% random coil) has become predominantly β-sheet (∼45%) and to a lesser extent α-helix (∼15%). Such a phenomenon has been reported in the context of Alzheimer and prion peptides (*43*, *44*).

In summary, our results give direct proof that preassembly of positively charged antimicrobial peptides increases their amphipathic structure, which in turn increases their activity toward zwitterionic membranes and therefore affects their target cell specificity.

REFERENCES

1. Boman, H. G. (1995) *Annu. Rev. Immunol. 13*, 61−92.
2. Nicolas, P., and Mor, A. (1995) *Annu. Rev. Microbiol. 49*, 277−304.
3. Lehrer, R. I., and Ganz, T. (1999) *Curr. Opin. Immunol. 11*, 23−27.
4. Hoffmann, J. A., Kafatos, F. C., Janeway, C. A., and Ezekowitz, R. A. (1999) *Science 284*, 1313−1318.
5. Hancock, R. E., and Diamond, G. (2000) *Trends Microbiol 8*, 402−410.
6. Zasloff, M. (2000) *Trends Pharmacol. Sci. 21*, 236−238.
7. Matsuzaki, K. (1999) *Biochim. Biophys. Acta 1462*, 1−10.
8. Shai, Y. (1999) *Biochim. Biophys. Acta 1462*, 55−70.
9. Bechinger, B. (1999) *Biochim. Biophys. Acta 1462*, 157−183.
10. Dathe, M., and Wieprecht, T. (1999) *Biochim. Biophys. Acta 1462*, 71−87.
11. Blondelle, S. E., Lohner, K., and Aguilar, M. (1999) *Biochim. Biophys. Acta 1462*, 89−108.
12. Epand, R. M., and Vogel, H. J. (1999) *Biochim. Biophys. Acta 1462*, 11−28.
13. Zhang, L., Scott, M. G., Yan, H., Mayer, L. D., and Hancock, R. E. (2000) *Biochemistry 39*, 14504−14514.
14. Tossi, A., Sandri, L., and Giangaspero, A. (2000) *Biopolymers 55*, 4−30.
15. Strahilevitz, J., Mor, A., Nicolas, P., and Shai, Y. (1994) *Biochemistry 33*, 10951−10960.
16. Ghosh, J. K., Shaool, D., Guillaud, P., Ciceron, L., Mazier, D., Kustanovich, I., Shai, Y., and Mor, A. (1997) *J. Biol. Chem. 272*, 31609−31616.
17. Oren, Z., Lerman, J. C., Gudmundsson, G. H., Agerberth, B., and Shai, Y. (1999) *Biochem. J. 341*, 501−513.
18. Oren, Z., and Shai, Y. (2000) *Biochemistry 39*, 6103−6114.
19. Feder, R., Dagan, A., and Mor, A. (2000) *J. Biol. Chem. 275*, 4230−4238.
20. Avrahami, D., Oren, Z., and Shai, Y. (2001) *Biochemistry 40*, 12591−12603.
21. Allen, T. M., and Cleland, L. G. (1980) *Biochim. Biophys. Acta 597*, 418−426.
22. Sims, P. J., Waggoner, A. S., Wang, C. H., and Hoffman, J. F. (1974) *Biochemistry 13*, 3315−3330.
23. Gazit, E., Boman, A., Boman, H. G., and Shai, Y. (1995) *Biochemistry 34*, 11479−11488.
24. Rothemund, S., Beyermann, M., Krause, E., Krause, G., Bienert, M., Hodges, R. S., Sykes, B. D., and Sonnichsen, F. D. (1995) *Biochemistry 34*, 12954−12962.
25. Mozsolits, H., Wirth, H. J., Werkmeister, J., and Aguilar, M. I. (2001) *Biochim. Biophys. Acta 1512*, 64−76.
26. Masson, L., Mazza, A., and Brousseau, R. (1994) *Anal. Biochem. 218*, 405−412.
27. MacKenzie, C. R., Hirama, T., Lee, K. K., Altman, E., and Young, N. M. (1997) *J. Biol. Chem. 272*, 5533−5538.
28. Verkleij, A. J., Zwaal, R. F., Roelofsen, B., Comfurius, P., Kastelijn, D., and van Deenen, L. L. (1973) *Biochim. Biophys. Acta 323*, 178−193.
29. Shaw, N. (1974) *Adv. Appl. Microbiol. 17*, 63−108.
30. Jackson, M., and Mantsch, H. H. (1995) *Crit. Rev. Biochem. Mol. Biol. 30*, 95−120.
31. Tatulian, S. A., Biltonen, R. L., and Tamm, L. K. (1997) *J. Mol. Biol. 268*, 809−815.
32. Dwivedi, A. M., and Krimm, S. (1984) *Biopolymers 23*, 923−943.
33. Krause, E., Beyermann, M., Dathe, M., Rothemund, S., and Bienert, M. (1995) *Anal. Chem. 67*, 252−258.
34. Sharon, M., Oren, Z., Shai, Y., and Anglister, J. (1999) *Biochemistry 38*, 15305−15316.
35. Pezolet, M., Bonenfant, S., Dousseau, F., and Popineau, Y. (1992) *FEBS Lett. 299*, 247−250.
36. Mantsch, H. H., Perczel, A., Hollosi, M., and Fasman, G. D. (1993) *Biopolymers 33*, 201−207.
37. Byler, D. M., and Susi, H. (1986) *Biopolymers 25*, 469−487.
38. Miyazawa, T. (1960) *J. Mol. Spectrosc. 4*, 168−172.
39. Schiffer, M., and Edmundson, A. B. (1967) *Biophys. J. 7*, 121−135.
40. Blondelle, S. E., and Houghten, R. A. (1992) *Biochemistry 31*, 12688−12694.
41. Oren, Z., Hong, J., and Shai, Y. (1997) *J. Biol. Chem. 272*, 14643−14649.
42. Hancock, R. E., and Rozek, A. (2002) *FEMS Microbiol. Lett. 206*, 143−149.
43. Symmons, M. F., Buchanan, S. G., Clarke, D. T., Jones, G., and Gay, N. J. (1997) *FEBS Lett. 412*, 397−403.
44. Gay, N. J., Packman, L. C., Weldon, M. A., and Barna, J. C. (1991) *FEBS Lett. 291*, 87−91.

BI0260482